An auxetic meta-structure enabled soft locomotive robot

Check for updates

Peng Jiang[1], Yang Deng[1], Xiaoyi Wang[1,2], Qian Xu[1], Rui Jiao[1] & Hongyu Yu[1] ✉

This paper introduces the ADAMBOT, a novel soft locomotive robot that leverages the active deformability of auxetic meta-structures, a feature largely unexplored in robotics. The ADAMBOT utilizes a unique soft auxetic structure (SAS), combining rigid boxes with elastic joints, enabling it to achieve both the compliance of soft materials and the properties of auxetic meta-structures. Driven by a single motor and multi-electromagnet hybrid drive system, the ADAMBOT achieves planar motion on ferromagnetic surfaces through actuation-induced body deformation, leveraging electromagnets for adhesion. This design enables the ADAMBOT to transition seamlessly from ground to curved surfaces and then to vertical walls, demonstrating exceptional adaptability. The ADAMBOT can cross gaps between two surfaces, showcasing its potential for navigating challenging terrains. Its reconfigurable design allows for rapid assembly into different configurations, adapting to diverse tasks. The ADAMBOT's capabilities demonstrate the potential of robots based on SAS for exploration and detection in challenging and unfamiliar environments, opening up new possibilities for robotics in diverse applications.

The pursuit of machines capable of navigating complex and unpredictable terrains fuels the rapid evolution of the robotics field. Researchers have developed a diverse array of locomotive robots tailored to specific terrains, including wheeled robots[1–4], tracked robots[5,6], legged robots[7,8], flying robots[9,10] and underwater robots[11–13]. While traditional rigid robots excel in structured settings, their limitations become apparent when confronted with unstructured terrains, obstacles, and dynamic environments. To enhance the adaptability of locomotive robots to unstructured terrains, some researchers have developed wheel-legged robots[14,15]. This challenge has also spurred the development of soft locomotive robots, which utilize compliant materials and designs to achieve greater flexibility, adaptability, and resilience. Soft locomotive robots[16–22] have shown promise in various applications, ranging from minimally invasive surgery and search and rescue operations to human-robot interaction and environmental monitoring.

A particularly intriguing class of materials for soft robotics are auxetic structures, known for their negative Poisson's ratio[23–27]. This unique property distinguishes them from conventional materials, which contract in the transverse direction when stretched longitudinally. Auxetic materials, on the other hand, expand in the transverse direction when subjected to longitudinal tension. Notably, auxetic meta-structures have also been investigated in kirigami-based metamaterials, where tailored cuts and geometric patterns enable programmable deformation and tunable mechanical responses[28–31]. This unusual behavior has led to their exploration

in various applications, including robotics[32–39], aerospace[40], biomedical engineering[41], etc.

Current research efforts have explored the use of auxetic structures in soft robotics[30–33], demonstrating their potential for achieving controlled deformation and locomotion. However, existing implementations often face limitations. Many auxetic structures, while exhibiting desirable properties, lack the necessary softness for navigating complex and delicate terrains. Additionally, many designs rely on external power sources, such as compressed air[31], limiting their autonomy and practicality in real-world scenarios.

The potential of auxetic structures for active deformation and locomotion in robotics remains largely unexplored. One particularly promising type of auxetic structure for robotics is the rotating quadrangular rigid auxetic meta-structure[25,27] (Fig. 1A). This structure exhibits a unique ability to translate in-situ deformation into global deformation, allowing for controlled and predictable movement. Leveraging this characteristic, controlled displacement of the entire structure can be achieved by immobilizing a specific structural unit during deformation processes (Fig. 1B). Referring to the electromagnet-based soft locomotive robot, the electromagnets can be installed in the characteristic elements of the auxetic meta-structure, and its continuous movement on the ferromagnetic surface can be controlled. Drawing inspiration from electromagnet-based soft locomotive robots[42,43], electromagnets could be integrated into the characteristic elements of the auxetic meta-structure to enable controlled and continuous movement on

[1]Department of Mechanical and Aerospace Engineering, The Hong Kong University of Science and Technology, Hong Kong, China. [2]The School of Integrated Circuits and Electronics, Beijing Institute of Technology, Beijing, China. ✉e-mail: hongyuyu@ust.hk
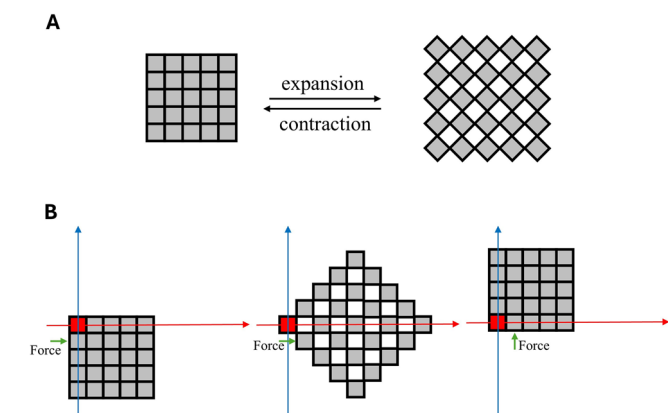
A

B

Fig. 1 | Rotating quadrangular auxetic meta-structure. A Expansion and contraction states of the rotating square auxetic meta-structure. B The rotating square auxetic meta-structure's displacement is shown when the red square unit is held in place. Pushing a single unit caused deformation of the entire structure.

ferromagnetic surfaces. However, its deformation is fundamentally constrained by the 2D rotational coupling mechanism, which restricts motion to the structural plane and inhibits out-of-plane bending or torsional actuation required for complex robotic behaviors.

This paper introduces the ADAMBOT, a novel soft locomotive robot that utilizes a type of rotating square auxetic meta-structure for locomotion. The ADAMBOT's design integrates rigid boxes connected by elastic joints, forming a soft auxetic structure (SAS) that exhibits both the properties of soft materials and auxetic meta-structures. This allows the ADAMBOT to achieve planar motion on ferromagnetic surfaces through actuation-induced body deformation, leveraging electromagnets for adhesion. Notably, the ADAMBOT achieves this planar locomotion using a single motor and multi-electromagnet hybrid driving system, a significant departure from conventional robots that rely on multiple motors and complex transmission mechanism for complex movements. This hybrid driving system design simplifies control, reduces structural complexity, and potentially lowers cost.

This paper will delve into the design, fabrication, and experimental validation of the ADAMBOT, highlighting the advantages of its unique SAS, which enables planar motion with single motor and multi-electromagnet hybrid driving system and facilitates navigation of challenging terrains. We will explore the unique properties of auxetic meta-structures and their application in soft robotics, demonstrating the potential of this novel approach for exploration and detection in challenging and unfamiliar terrains. We will analyze the ADAMBOT's performance in various scenarios, showcasing its ability to navigate multi-terrain surfaces and perform specialized tasks. The results of our investigations will provide valuable insights into the potential of soft robots based on auxetic meta-structures, offering a new perspective for future mobile robot design.

Results
Motion principle of rotating rigid auxetic meta-structure
Rotating quadrangular plate structure is a type of 2D rotating rigid auxetic meta-structure[25–27]. It is composed of several quadrangular plate units interconnected via hinged joints. Similar to other auxetic structures, the SAS exhibits a negative Poisson's ratio; in this specific design, the Poisson's ratio value is −1. When the structure is subjected to compression or expansion along one principal axis, the interconnected quadrangular units undergo a coordinated rotational motion, which simultaneously induces complementary deformation along the orthogonal directions. During this process, if a single quadrangular unit within the auxetic structure is constrained, the entire system will exhibit rotational expansion or contraction of the unit (Fig. 1B). Concurrently, by altering the angle between any two adjacent units, the overall structure will undergo corresponding expansion or

contraction motions in correlation with the angular change. Leveraging these two distinctive characteristics, the rotating quadrangular plate structure can achieve planar locomotion by actively adjusting the angles between any neighboring units while selectively constraining a specific unit in the plane.

SAS design
The SAS is designed based on the rotating square plate structure. This structure is a specialized variant of the rotating quadrangular plates auxetic meta-structure, comprising numerous interconnected square units of uniform dimensions linked via hinge joints (Fig. 2C). A unique aspect of this configuration is the uniform expansion and contraction rates exhibited in different directions.

In the design process of the SAS, square boxes were employed as modular components instead of flat square plates. These boxed units provide ample internal volume to house various accessories, such as actuators and power sources. More importantly, replacing the original rigid hinges with compliant joints fabricated from thermoplastic polyurethane (TPU) (Fig. 2A) not only preserves the auxetic characteristics but introduces multiaxial compliance - enabling simultaneous in-plane deformation (X/Y-axis) and out-of-plane flexibility (Z-axis). This 3D compliance empowers passive obstacle negotiation through localized elastic deformation (Fig. 2D, E), terrain adaptation via curvature-matching mechanics, and enhanced structural survivability via viscoelastic damping of impact loads[44,45]. Furthermore, pre-tensioning the TPU joints during assembly synergizes with chamfered connection surfaces (Fig. 2B) to create geometric bistability, where stored elastic energy autonomously restores the metastructure to its maximum expanded configuration after compression, effectively preventing jamming failures inherent in rigid-hinge systems while maintaining positional stability absent external disturbances.

To further understand the mechanical behavior of the compliant joints, we conducted a stress and strain simulation of the elastic lines (Fig. 3A, B). In this simulation, the elastic lines were subjected to varying pre-stretch levels ranging from 1 to 1.5 times their original length. The resulting stress-strain curves (Fig. 3C) demonstrate how different pre-stretch levels influence the mechanical response of the elastic lines. This analysis emphasizes the significance of pre-stretching in optimizing force distribution within the SAS, thereby ensuring both flexibility and stability during operation.

Robot design
Based on the SAS, we developed a single-drive robot, ADAMBOT. The robot is composed of five subsystems: a SAS body, a pair of electromagnet feet, a drive module, a steering module and a control module. Although a SAS with a 2 × 2 configuration can achieve planar movement, we chose a 3 × 3 configuration for the ADAMBOT's body to ensure stability in its heading during motion. This configuration prevents the robot's head from rotating, which would occur with a 2 × 2 setup (Fig. 4A, C). The SAS body of the robot utilizes a standardized design approach, wherein all SAS units, with the exception of the three specialized units serving as the footpads and steering module, are identical in their configuration. This design approach confers ADAMBOT with attributes of facile installation and scalability, enabling users to assemble varied configurations tailored to distinct task requirements. Furthermore, the ADAMBOT's body structure incorporates only six dedicated component-housing units for essential elements such as motors and batteries, while the remaining vacant units can be utilized for accommodating additional payloads. As the overall configuration scale increases, the proportion of these unoccupied units increases substantially, with a 3 × 3 configuration ADAMBOT possessing three vacant units, and a 5 × 5 configuration ADAMBOT featuring nineteen such empty units.

Four electromagnets are divided into two groups and installed in the outermost two units of SAS body. They are two feet of the robot, which allows ADAMBOT to adhere and move on ferromagnetic surfaces. The drive module contains a DC motor, two high-tensile lines and a pulley. By

Fig. 2 | Compliant joint and force analysis.
A Composition of the compliant joint. **B** Working principle of the compliant joint. **C** Assembly of two square units. **D** Force analysis of square units and units with a curved shell while stepping over a small obstacle. **E** Force analysis of the ADAMBOT as it steps over a gap.
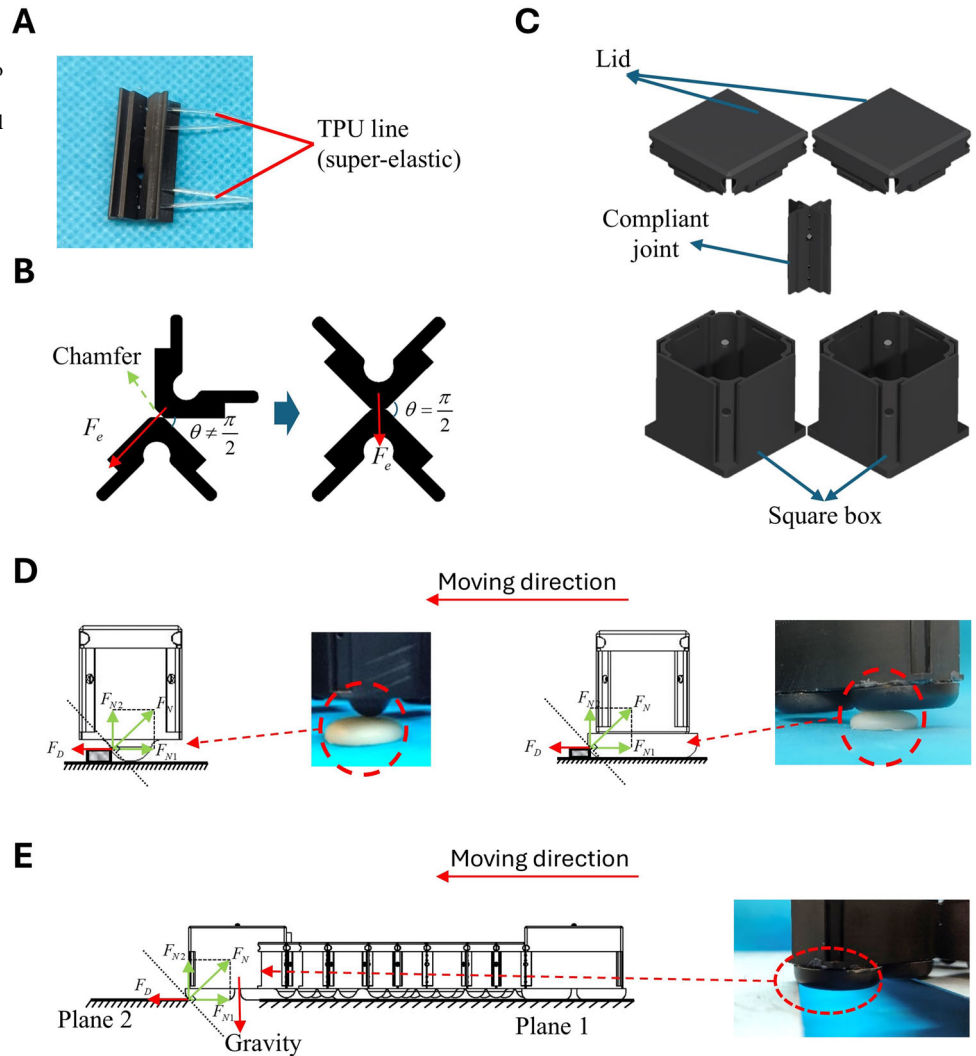
changing the number of twists of the high-tensile lines on the pulley, the motor can drive two adjacent squares to rotate, thus achieving contraction and expansion. The steering module contains only one electromagnet, which, in conjunction with the drive module, can be used to control the directional orientation of the robot's head. A Seeed XIAO microcontroller has been used in the robot's control module; users can control ADAMBOT remotely through a remote control (Fig. 4B). By controlling the on/off states of the electromagnets, as well as the direction of rotation and the number of turns of the motor, ADAMBOT can achieve effective planar motion (Fig. 4C).

ADAMBOT operates on a planar surface using a sliding motion, which results in significant frictional forces during movement. To reduce the frictional forces encountered while moving, the bottom of the square units is designed with a hemispherical structure (Fig. 2D). This design minimizes the contact area between the units and the surface, effectively reducing friction. Additionally, this design offers the advantage of enabling these units to navigate terrains with small obstacles, holes, and cracks. For units equipped with electromagnets, such as the robot's feet, which may be obstructed by obstacles, we have designed a casing with a curved outer surface (Fig. 2E). This enables ADAMBOT to navigate complex terrains with obstacles, cracks, or small pits.

Motion analysis
For a robot based on SAS, the maximum stride length depends on the structure's area expansion rate and the unit's side length. As a rotating square structure, the area expansion ratio β of SAS is constant.

$$\beta = \frac{Area_{expansion} - Area_{contraction}}{Area_{contraction}} = \frac{n\sqrt{2}a * m\sqrt{2}a - na * ma}{na * ma} = 100\%$$

(1)

where n is the number of rows, m is the number of columns, and a is the side length of square units (Fig. 5A). For an $n*m$ configuration robot, choose the two square units at each end of the diagonal as the feet of the robot. The distance D between the two square units can be represented as follows:

$$D = \sqrt{d_x^2 + d_y^2}$$

(2)

$$d_x = \frac{a}{2}[(n + m) + (n + m)sin\theta + (n - m)cos\theta]$$

(3)

$$d_y = \frac{a}{2}[(m - n) + (m - n)sin\theta + (n + m)cos\theta]$$

(4)

Where θ is the angle between two adjacent square units, and its value range is $0 \le \theta \le \pi$, a is the edge length of the square units.

The value of the angle θ depends on the length of the two high-tensile lines l_1, l_2 between the two units in the drive system, as shown in Fig. 5C. Two

Fig. 3 | Stress simulation of the elastic lines in compliant joints. A Stress distribution in one of the joints when the elastic line is not pre-stretched, with a rotation angle of 56 degrees. **B** Stress distribution in one of the joints when the pre-stretched length of the elastic line is 1.5 times its original length, also at a rotation angle of 56 degrees. **C** Stress curves of the elastic lines in the joints under different pre-tension conditions during the contraction process of a 2×2 configuration SAS.
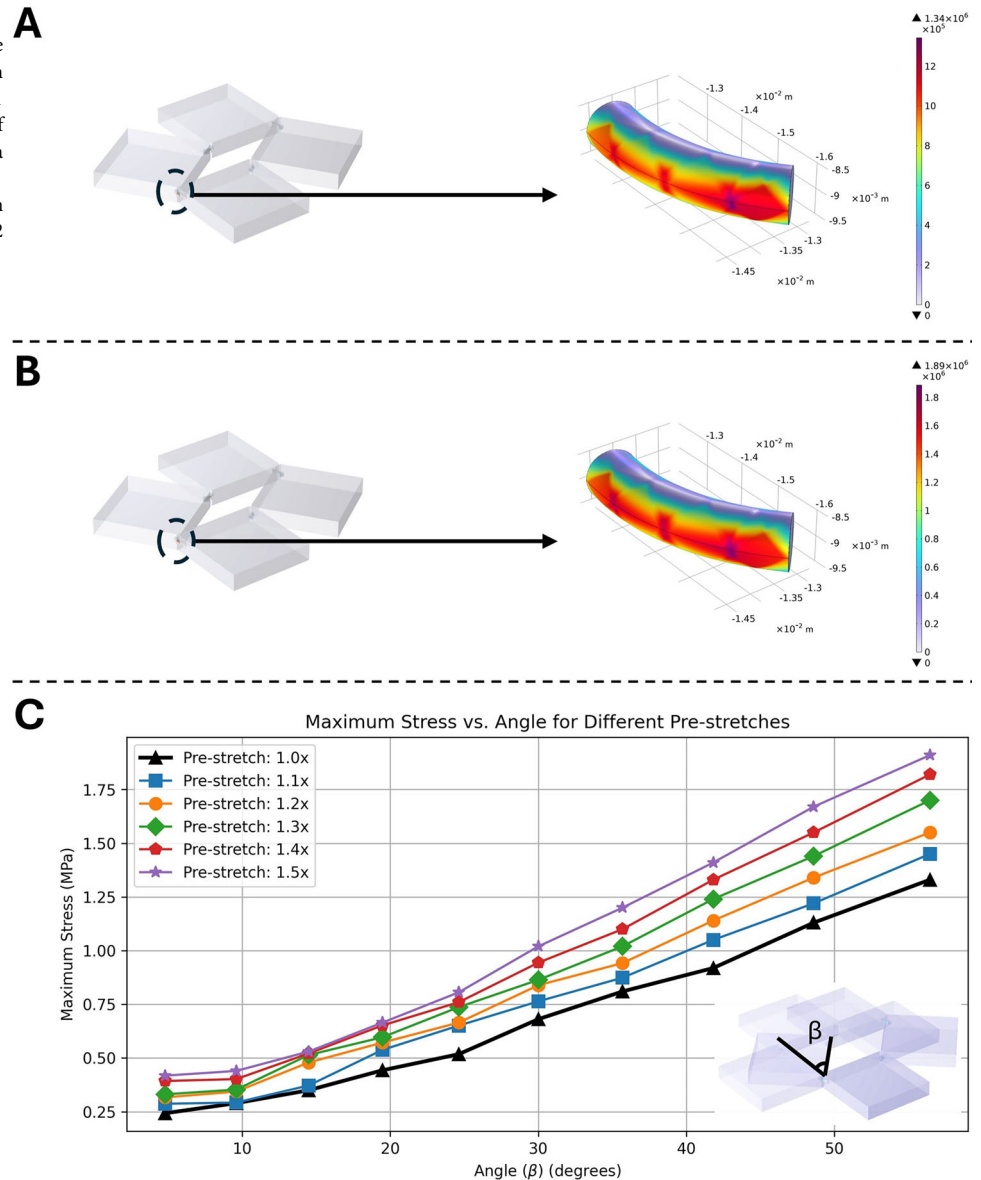
high-tensile lines are wound around a pulley in opposite directions, and the motor controls the pulley to rotate forward or backward. When the motor is working, it can drive one line to shorten and the other line to lengthen. Additionally, the radius of the pulley is the same where the two high-tensile lines are wound, so the elongation speed of one line is always the same as the shortening speed of the other.

As depicted in Fig. 4D, the relationship between the lines' length, vertex separation d_{p1p2} and d_{p3p4}, and included angle θ of the two square units, with the red line serving as the driving line, is illustrated. As the included angle θ increases from 0 to 180 degrees, the entire auxetic structure transitions from a fully contracted state to a fully expanded state, and then back to a fully contracted state. Depending on the relationship between the angle θ, vertex separation, and the lengths of the two lines, we have divided this process into six distinct stages, as depicted in Fig. 5C.

Experimental validation

To validate the capabilities of the ADAMBOT, we conducted a series of targeted tests in a controlled laboratory environment. Given the robot's requirement to move on ferromagnetic surfaces, we prepared several steel plates and a table with a ferromagnetic desktop surface to create the testing setup.

All experiments were performed using the ADAMBOT in a 3×3 configuration. The user interfaced with the robot via a smartphone device, controlling the ADAMBOT's operation through a Bluetooth connection to execute the required motions during the experimental trials.

Ground locomotion

In this experiment, a flat ferromagnetic metal plate with an area of 1000×500 mm was placed on a horizontally positioned table to demonstrate the ADAMBOT's ability to move across a horizontal surface. The experiment employed a manual control, with the operator using a mobile phone as the remote control unit to send control signals to the robot, guiding it to perform the required actions. This experiment verified the robot's ability to move in a plane, including translation and rotation in different directions.

Climbing verification

The ADAMBOT can climb on ferromagnetic walls; however, due to the elastic connection of the units inside the robot, it can only climb on surfaces with a slope angle of no more than 90 degrees. If ADAMBOT moves on a surface with a slope angle greater than 90 degrees, the elastic high-tensile lines in the elastic joints will stretch due to the robot's gravity. This stretching

Fig. 4 | Components, electronic architecture, and movement principles of the ADAMBOT.
A Installation of the 3×3 configuration ADAMBOT, showing: (1) electromagnet, (2) curved shell for the electromagnet, (3) DC motor, (4) compliant joints, (5) battery, (6) drive line, and (7) Seeed XIAO development board. **B** Electronic architecture of the ADAMBOT. **C** Principles for achieving different movements.
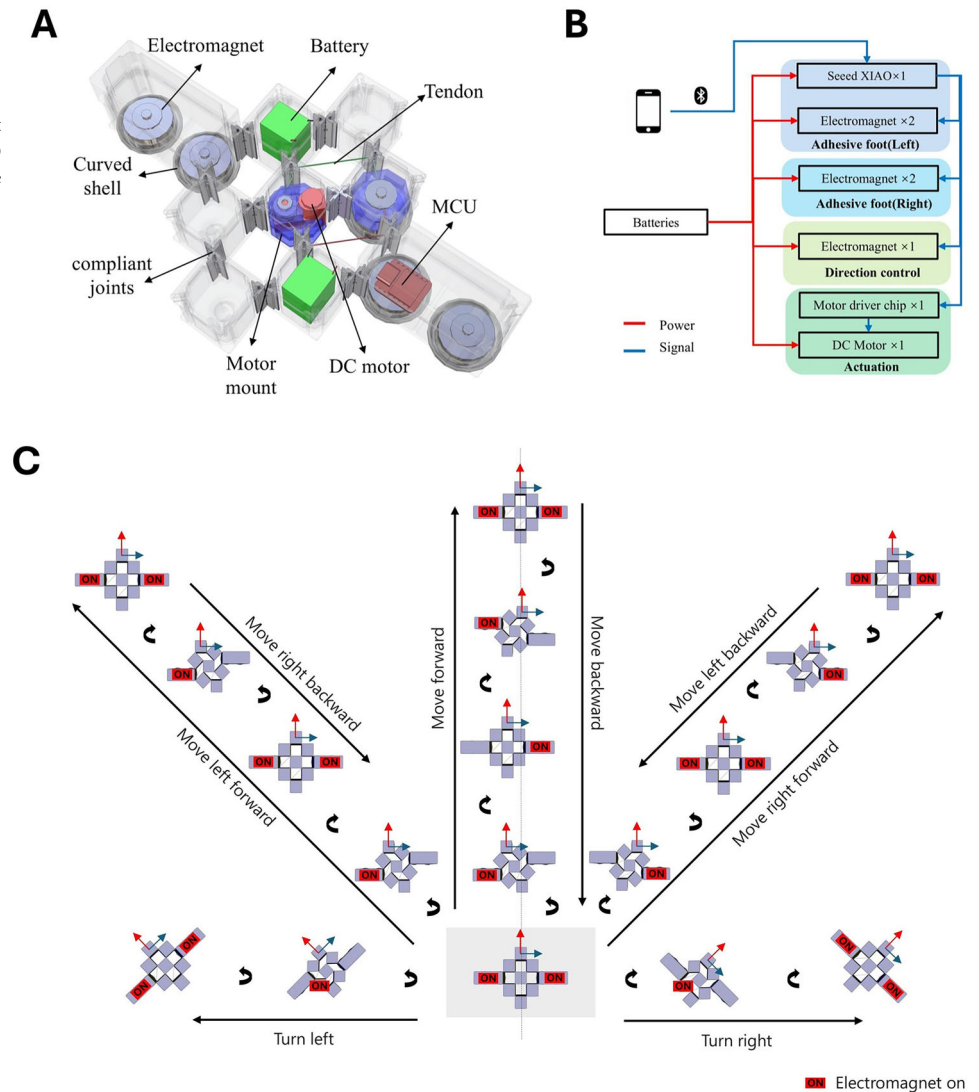
will cause the electromagnet to detach from the wall when powered off and prevent it from reattaching after being powered on again.

For the purposes of this experimental study, a flat ferromagnetic metal plate was taken as the test surface and placed perpendicular to the ground. Under manual control mode, the robotic system successfully executed the actions required by the experimental protocol, including climbing upwards, climbing downwards, and horizontal translation across the test surface (Fig. 6A).

Multi-plane transition capabilities

To evaluate the ADAMBOT's versatility in navigating diverse surface orientations, we conducted experiments assessing its multi-plane transition capabilities. The robot, measuring 213 mm by 137 mm in its fully expanded configuration, successfully traversed a sequence of surfaces with varying geometries, including a horizontal plane, a curved section, and a vertical surface (Fig. 6B). Through remote control, the ADAMBOT demonstrated the ability to seamlessly transition between these different surface orientations.

Building on this, the ADAMBOT was challenged to step over a 30 mm gap between two horizontal surfaces, a task that exceeded the size of its individual body components (28 mm) (Fig. 7B). Leveraging its unique SAS body, the robot was able to successfully traverse the discontinuous planes, distinguishing it from many wall-climbing robots that struggle with such surface discontinuities.

Navigating challenging terrains

To further evaluate the ADAMBOT's mobility capabilities, we assessed its performance across diverse and demanding surface conditions. The robot, with a height of 49.5 mm, successfully navigated a ferromagnetic terrain featuring obstacles, pits, and uneven features. Additionally, the ADAMBOT exhibited remarkable stability and control on wet and vibrating ferromagnetic surfaces, seamlessly adapting its gait and adhesion mechanisms to the changing conditions.

The ADAMBOT's compact design also enabled it to navigate through narrow gaps and confined spaces, traversing a 60 mm gap without issue. This capability to operate in constrained terrains expands the robot's potential applications, allowing it to access and navigate areas inaccessible to larger robotic systems.

Collectively, these findings highlight the ADAMBOT's robust and adaptable design, positioning it as a viable candidate for a wide range of applications requiring advanced mobility and adaptability.

Demonstration of route tracking

To further showcase the ADAMBOT's navigation capabilities, we conducted a demonstration of route tracking. An ArUco marker was glued on the ADAMBOT, allowing for reliable detection and tracking of the robot's position and orientation using an OpenCV-based program. As the user-guided the ADAMBOT through a pre-defined route spelling out the letters "HKUST," the real-time visualization of the robot's trajectory on a display
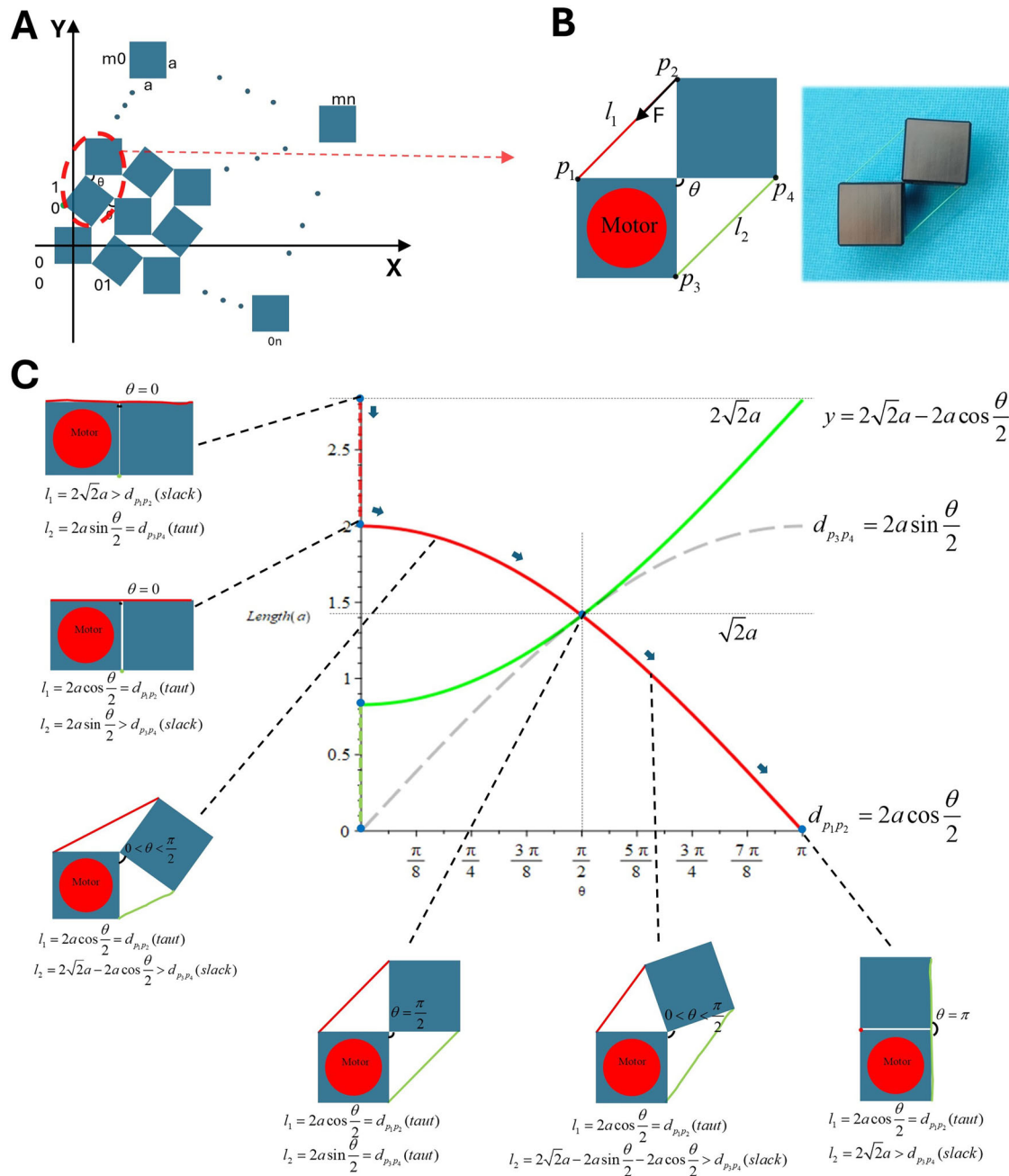
Fig. 5 | Kinematics analysis. A Model of a rotating squares auxetic structure with n rows and m columns. **B** Schematic diagram and prototype of the ADAMBOT's drive system. **C** Variation of the lengths of two high-tensile lines with the angle θ from 0 to π. Red indicates the line in drive mode, while green indicates the line in non-drive mode. This section illustrates the movement of the drive system as the angle θ increases from 0 to π, along with the relationship between the line lengths l_1 and l_2 and the distances d_{p1p2} and d_{p3p4}.

highlighted its exceptional stability, responsiveness, and adherence to the desired path (Fig. 7C). This demonstration underscored the ADAMBOT's versatility and suitability for applications requiring precise, controlled, and visually traceable movements.

Loading test

To evaluate the ADAMBOT's load capacity, a dedicated loading test was conducted. Compared to other robots, the ADAMBOT's modular design provides ample interior space for accommodating additional payloads, offering protection and increasing the overall load capacity.

The ADAMBOT in its fully expanded 3×3 configuration, with 3 onboard batteries, has a self-weight of 310.6 g. For the loading test on a horizontal surface, we used 100-g weights that could be housed within the

robot's body units. Experiments on a horizontal ferromagnetic surface showed the ADAMBOT could carry a maximum load of 1000 g, which is more than three times its own weight (Fig. 8A).

In addition, tests performed on a vertical surface revealed that the ADAMBOT can support a maximum load of 300 g (Fig. 8B). This capability illustrates the robot's exceptional load capacity and its suitability for applications requiring the transport of substantial payloads in both horizontal and vertical orientations.

Discussion

Soft locomotive robots represent a significant advancement in the field of robotics, characterized by their use of flexible, deformable materials that enable them to navigate complex and dynamic terrains with ease. Unlike

Fig. 6 | ADAMBOT movement demonstration.
A Climbing demonstration of the ADAMBOT.
B Transition of the ADAMBOT from a horizontal surface to a curved surface and then to a vertical surface. All surfaces are ferromagnetic.
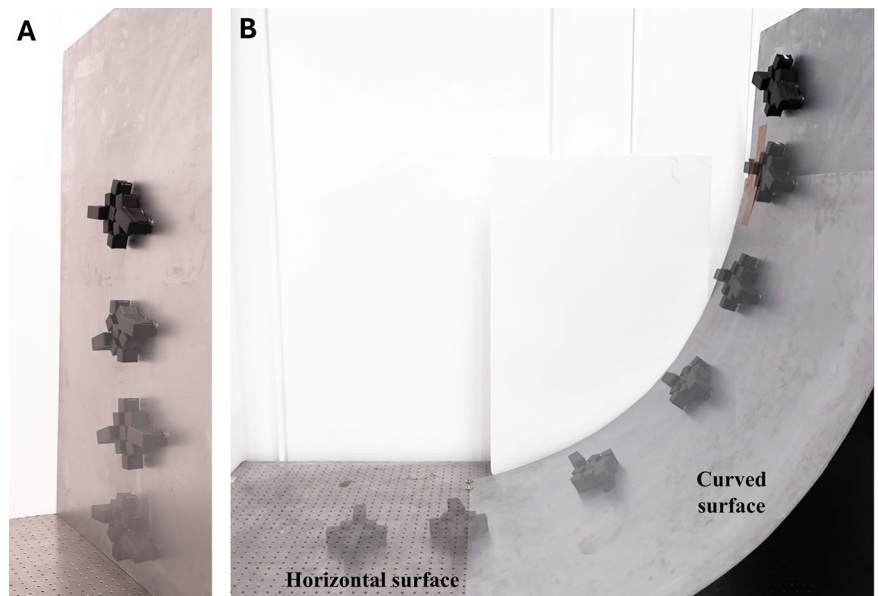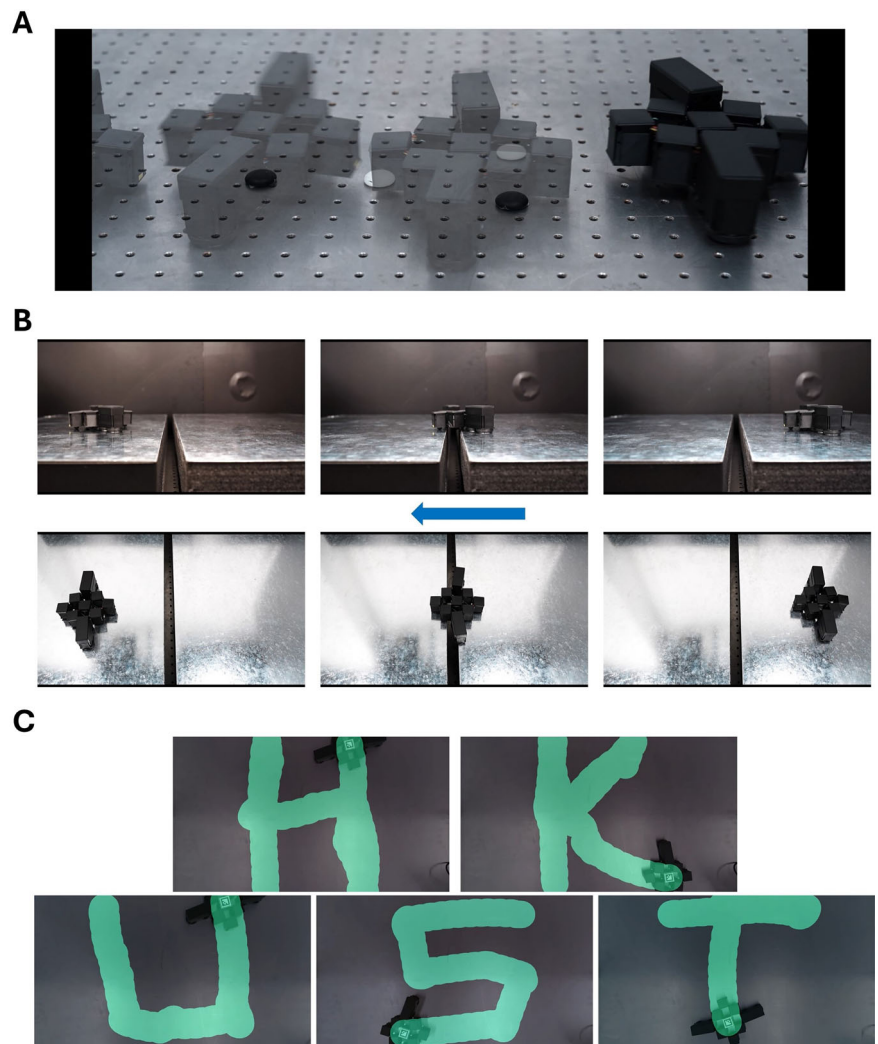

Fig. 7 | ADAMBOT movement capabilities.
A ADAMBOT navigating a surface with obstacles (Go stones, diameter 22 mm, height 6.5 mm) and holes (diameter 6 mm). **B** ADAMBOT stepping over a 30 mm gap between two surfaces. **C** User-controlled route tracking of five letters.
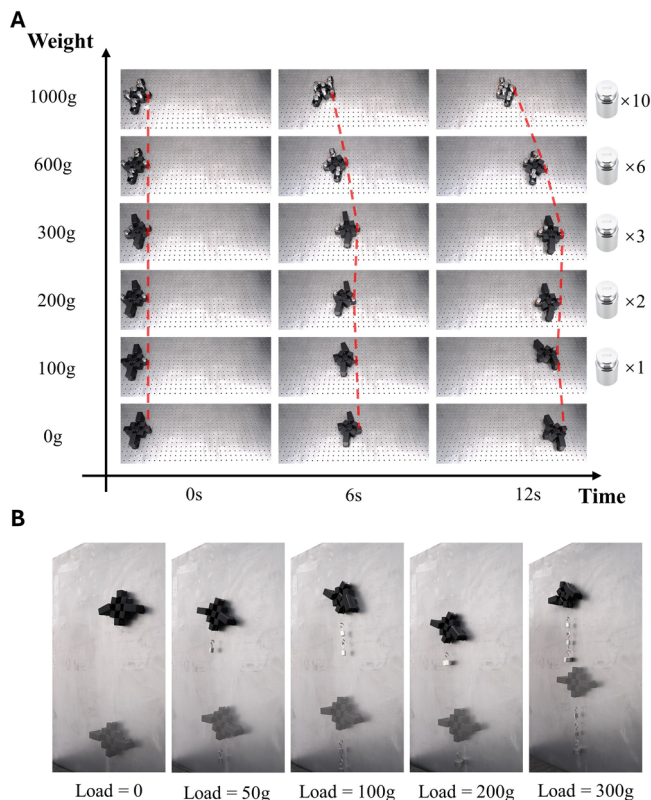
Fig. 8 | ADAMBOT loading tests. A Load test of the robot on a horizontal surface. **B** Load test of the robot on a vertical surface.

rigid-bodied robots, soft robots can adapt their shape to traverse uneven terrain, squeeze through tight spaces, and interact safely with delicate objects and humans. This inherent flexibility offers numerous advantages, including enhanced adaptability, reduced risk of damage, and improved safety in human-robot interactions. Despite these promising developments, several challenges remain. The control and actuation of soft robots are more complex compared to traditional rigid robots, requiring sophisticated algorithms and advanced materials. Furthermore, ensuring the durability and reliability of soft robots in harsh conditions is an ongoing research focus. ADAMBOT tries to use innovative materials, SAS, and hybrid design to combine the benefits of soft and rigid components to overcome these limitations. However, the robot still faces its own challenges.

The proposed SAS design leverages the principles of rotating square auxetic meta-structures, offering a unique approach to achieving adaptable and compliant robotic systems. Unlike traditional auxetic structures that rely on rigid hinge joints[39–41], the SAS incorporates compliant joints designed with elastic materials. This departure from traditional inextensible hinge connections endows the SAS with a remarkable degree of flexibility, transforming it into a compliant structure capable of adapting to multiterrain surfaces.

The compliant nature of the SAS, enabled by TPU hinge elasticity, introduces critical functional advantages. First, the multi-axis compliance (Z-axis flexibility and X/Y-axis auxetic motion) allows passive terrain adaptation, where localized hinge deformation absorbs irregular surface impacts (e.g., cracks, protrusions) while maintaining structural integrity. Second, the viscoelastic damping of TPU reduces peak stress under dynamic loads compared to rigid hinges, enhancing survivability in collision-prone environments. Finally, the pre-tensioned hinge design enables autonomous shape recovery after compression, eliminating mechanical deadlocks inherent in rigid systems. Additionally, this inherent feature provides ample internal space for housing additional payloads, actuators, and power sources, crucial for enhancing the functionality and capabilities of the robot.

Furthermore, the modular design of the SAS allows for easy scalability. The number of structural units can be readily adjusted without altering other system components, enabling the creation of robots with different sizes to suit specific tasks. However, with increasing size, a single drive module may face challenges in effectively driving the entire structure. This issue can be addressed by incorporating multiple drive modules, ensuring efficient operation even for larger-scale robots.

The innovative combination of auxetic meta-structures and compliant joints in the SAS design presents a promising avenue for developing adaptable and flexible robotic systems. The inherent space-saving features and modular design of the SAS offer significant advantages for various applications, while the challenges associated with driving larger-scale structures can be addressed through the integration of multiple drive modules. Future research will focus on further exploring the potential of the SAS design, optimizing its performance, and addressing the challenges associated with its implementation in real-world scenarios.

A key challenge in the ADAMBOT's design arises from movement errors caused by elastic joint deformation. Variations in surface friction can lead to discrepancies between intended and actual trajectories, propagating inaccuracies through the control system and limiting precision-critical tasks. Additionally, the current electromagnet-based adhesion restricts operation to ferromagnetic surfaces, reducing versatility in non-magnetic environments.

To address these limitations, advanced sensing and control algorithms could mitigate elastic deformation effects by dynamically compensating for environmental variability. Furthermore, exploring alternative adhesion strategies—such as gecko-inspired dry adhesives or suction-based systems—would broaden the ADAMBOT's operational scope to diverse substrates. By refining adaptability while preserving precision, this soft-rigid hybrid approach holds promise for deployment in complex, dynamic settings.

The ADAMBOT integrates soft robotics' flexibility with rigid components' precision, employing elastic joints and shape-adaptable structures to navigate challenging terrains. While its current electromagnet adhesion limits surface compatibility, ongoing efforts to develop multifunctional adhesion mechanisms aim to unlock broader applications, from industrial inspection to search-and-rescue operations.

Methods

Design and fabrication of the ADAMBOT

The ADAMBOT's rigid components are fabricated using Digital Light Processing (DLP) technology, employing an environmentally friendly ANYCUBIC Plant-Based Resin. Each compliant joint comprises three components: two identical 3D-printed parts tied by an elastic line made of TPU. Snap-on or latch-type connections between components facilitate easy assembly and disassembly, eliminating the need for fasteners such as bolts and reducing overall weight.

All square box units have an external dimension of $28 \times 28 \times 36$ mm with a wall thickness of 1 mm. This dimension was chosen to accommodate the installation of the electromagnet, driver, and battery within the unit. The robot's two feet are designed using rectangular boxes with an external dimension of $66 \times 28 \times 49.5$ mm. This design provides greater internal space for the installation of two electromagnets and other electronic components. The integration of two electromagnets within each foot unit aims to prevent the robot from rotating around the attachment point due to gravitational forces when carrying heavy loads or performing climbing movements.

Actuation and control system

A DC geared motor (N20) was selected to drive ADAMBOT. This motor has a rated power of 0.72W and provides a maximum torque of 0.088 N.m. Electromagnets with a diameter of 25mm and a height of 11mm were chosen as the suction units, each with a power rating of 1.8W and a maximum suction force of 49N. For control, a Seeed XIAO BLE development

board was selected. Users can send control signals to the development board via Bluetooth using a remote control to control the motor rotation and electromagnet activation, thereby controlling the robot's movement. Additionally, two sets of lithium polymer batteries are installed within the robot to provide power.

The ADAMBOT system employs a hybrid actuation architecture combining a single motor with multiple electromagnets, presenting distinct advantages and limitations compared to conventional multi-actuator configurations. While this design simplifies control logic through binary electromagnetic switching (on/off states) and enables vertical surface mobility via magnetic adhesion forces up to 9.8 N/cm^2, it introduces trade-offs in power density and mass distribution. Specifically, each electromagnet consumes 1.8 W during activation—significantly higher than the 0.72 W of the motor—while contributing around 40% of the system's total weight. Alternative multi-actuator implementations, such as pneumatic adhesion systems requiring pressure differentials or active friction modulation mechanisms, often demand additional subsystems that compromise structural compactness. Nevertheless, the current modular design facilitates rapid reconfiguration and provides inherent scalability for functional expansion. Future developments will focus on contact interface optimization to reduce electromagnetic dependency through bistable adhesion mechanisms.

Data availability

Data supporting the findings of this study are available in the Article and its Supplementary Information and by request from the Authors.

References

1. Lee, J.-Y. et al. Variable-stiffness–morphing wheel inspired by the surface tension of a liquid droplet. *Sci. Robot.* **9**, eadl2067 (2024).
2. Kim, G., Chung, H. & Cho, B.-K. Mobinn: Stair-climbing mobile robot with novel flexible wheels. *IEEE Trans. Ind. Electron.* **71**, 9182–9191 (2023).
3. Zheng, C., Sane, S., Lee, K., Kalyanram, V. & Lee, K. α-waltr: adaptive wheel-and-leg transformable robot for versatile multiterrain locomotion. *IEEE Trans. Robot.* **39**, 941–958 (2023).
4. Fu, Q., Guan, Y., Liu, S. & Zhu, H. A novel modular wheel-legged mobile robot with high mobility. In *2021 IEEE International Conference on Robotics and Biomimetics (ROBIO)*, 577–582 (2021).
5. Li, Z., Jing, X., Sun, B. & Yu, J. Autonomous navigation of a tracked mobile robot with novel passive bio-inspired suspension. *IEEE/ASME Trans. Mechatron.* **25**, 2633–2644 (2020).
6. Wang, W., Zhou, L., Du, Z. & Sun, L. Track-terrain interaction analysis for tracked mobile robot. In *2008 IEEE/ASME International Conference on Advanced Intelligent Mechatronics*, 126–131 (2008).
7. Chen, T. et al. Design and control of a novel leg-arm multiplexing mobile operational hexapod robot. *IEEE Robot. Autom. Lett.* **7**, 382–389 (2022).
8. Mahkam, N., Bakir, A. & özcan, O. Miniature modular legged robot with compliant backbones. *IEEE Robot. Autom. Lett.* **5**, 3923–3930 (2020).
9. Xiao, S., Hu, K., Huang, B., Deng, H. & Ding, X. A review of research on the mechanical design of hoverable flapping wing micro-air vehicles. *J. Bionic Eng.* **18**, 1235–1254 (2021).
10. Wood, R. J. The first takeoff of a biologically inspired at-scale robotic insect. *IEEE Trans. Robot.* **24**, 341–347 (2008).
11. Parra Rubio, A. et al. Modular morphing lattices for large-scale underwater continuum robotic structures. *Soft Robot.* **10**, 724–736 (2023).
12. Costa, D., Palmieri, G., Palpacelli, M.-C., Panebianco, L. & Scaradozzi, D. Design of a bio-inspired autonomous underwater robot. *J. Intell. Robotic Syst.* **91**, 181–192 (2018).
13. Masmitja, I. et al. Mobile robotic platforms for the acoustic tracking of deep-sea demersal fishery resources. *Sci. Robot.* **5**, eabc3701 (2020).
14. Liu, X. et al. Development of wheel-legged biped robots: a review. *J. Bionic Eng.* **21**, 607–634 (2024).
15. Zhou, Q. et al. Max: a wheeled-legged quadruped robot for multimodal agile locomotion. *IEEE Transactions on Automation Science and Engineering* 1–21 (2023).
16. Wang, X. et al. Multimodal locomotion ultra-thin soft robots for exploration of narrow spaces. *Nat. Commun.* **15**, 6296 (2024).
17. Yue, T., Bloomfield-Gadêlha, H. & Rossiter, J. Snail-inspired water-enhanced soft sliding suction for climbing robots. *Nat. Commun.* **15**, 4038 (2024).
18. Dikici, Y., Daltorio, K. & Akkus, O. Nodes for modes: nodal honeycomb metamaterial enables a soft robot with multimodal locomotion. *Bioinspir. Biomim.* **19**, 046002 (2024).
19. Li, G. et al. Self-powered soft robot in the Mariana Trench. *Nature* **591**, 66–71 (2021).
20. Bartlett, N. W. et al. A 3d-printed, functionally graded soft robot powered by combustion. *Science* **349**, 161–165 (2015).
21. Shepherd, R. F. et al. Multigait soft robot. *Proc. Natl. Acad. Sci. USA* **108**, 20400–20403 (2011).
22. Ching, T. et al. Crawling, climbing, perching, and flying by fiba soft robots. *Sci. Robot.* **9**, eadk4533 (2024).
23. Lim, T.-C. *Auxetic Materials and Structures* Vol. 34 (Springer, 2015).
24. Yang, W., Li, Z.-M., Shi, W., Xie, B.-H. & Yang, M.-B. Review on auxetic materials. *J. Mater. Sci.* **39**, 3269–3279 (2004).
25. Ren, X., Das, R., Tran, P., Ngo, T. D. & Xie, Y. M. Auxetic metamaterials and structures: a review. *Smart Mater. Struct.* **27**, 023001 (2018).
26. Shukla, S. & Behera, B. Auxetic fibrous structures and their composites: a review. *Compos. Struct.* **290**, 115530 (2022).
27. Li, X., Peng, W., Wu, W., Xiong, J. & Lu, Y. Auxetic mechanical metamaterials: from soft to stiff. *Int. J. Extrem. Manuf.* **5**, 042003 (2023).
28. Rafsanjani, A., Zhang, Y., Liu, B., Rubinstein, S. M. & Bertoldi, K. Kirigami skins make a simple soft actuator crawl. *Sci. Robot.* **3**, eaar7555 (2018).
29. Liu, Q. et al. Electronically configurable microscopic metasheet robots. *Nat. Mater.* **24**, 109–115 (2025).
30. Rafsanjani, A., Bertoldi, K. & Studart, A. R. Programming soft robots with flexible mechanical metamaterials. *Sci. Robot.* **4**, eaav7874 (2019).
31. Deng, Y. et al. Rotating square tessellations enabled stretchable and adaptive curved display. *npj Flex. Electron.* **8**, 4 (2024).
32. Lee, H. et al. 3d-printed programmable tensegrity for soft robotics. *Sci. Robot.* **5**, eaay9024 (2020).
33. Grossi, B., Palza, H., Zagal, J., Falcón, C. & During, G. Metarpillar: soft robotic locomotion based on buckling-driven elastomeric metamaterials. *Mater. Des.* **212**, 110285 (2021).
34. Chin, L. et al. Compliant electric actuators based on handed shearing auxetics. In *2018 IEEE International Conference on Soft Robotics (RoboSoft)*, 100–107 (IEEE, 2018).
35. Mark, A. G., Palagi, S., Qiu, T. & Fischer, P. Auxetic metamaterial simplifies soft robot design. In *2016 IEEE international conference on robotics and automation (ICRA)*, 4951–4956 (IEEE, 2016).
36. Chin, L., Burns, M., Xie, G. & Rus, D. Flipper-style locomotion through strong expanding modular robots. *IEEE Robot. Autom. Lett.* **8**, 528–535 (2022).
37. Lee, Y.-J. et al. Tendon-driven auxetic tubular springs for resilient hopping robots. *Adv. Intell. Syst.* **4**, 2100152 (2022).
38. Dikici, Y., Jiang, H., Li, B., Daltorio, K. A. & Akkus, O. Piece-by-piece shape-morphing: engineering compatible auxetic and non-auxetic lattices to improve soft robot performance in confined spaces. *Adv. Eng. Mater.* **24**, 2101620 (2022).

39. Liu, B. et al. Three-dimensional auxetic structure design methods based on bulking-induced deformation and the application in soft crawling robot. *Compos. B Eng.* **244**, 110146 (2022).

40. Budarapu, P., YB, S. S. & Natarajan, R. Design concepts of an aircraft wing: composite and morphing airfoil with auxetic structures. *Front. Struct. Civ. Eng.* **10**, 394–408 (2016).

41. Bhullar, S. K. et al. Design and fabrication of auxetic PCL nanofiber membranes for biomedical applications. *Mater. Sci. Eng. C* **81**, 334–340 (2017).

42. Hu, Q., Dong, E. & Sun, D. Soft modular climbing robots. *IEEE Trans. Robot.* **39**, 399–416 (2022).

43. Xu, Y., Xiao, B., Balakumar, L., Obstein, K. L. & Dong, X. Wireless millimeter-size soft climbing robots with omnidirectional steerability on tissue surfaces. *IEEE Robot. Autom. Lett.* **8**, 5720–5726 (2023).

44. Qiao, P., Yang, M. & Bobaru, F. Impact mechanics and high-energy absorbing materials. *J. Aerosp. Eng.* **21**, 235–248 (2008).

45. Du Bois, P., Kolling, S., Koesters, M. & Frank, T. Material behaviour of polymers under impact loading. *Int. J. Impact Eng.* **32**, 725–740 (2006).

Author contributions
H.Y.Y. proposed the concept, P.J., Y.D. and X.Y.W. performed the preliminary design of the robot, P.J. performed the detailed design, and experimental studies, carried out the analysis, and wrote the manuscript. Q.X. and R.J. conducted the simulation. H.Y.Y. supervised the work.

Competing interests
The authors declare no competing interests.

Additional information
Supplementary information The online version contains supplementary material available at https://doi.org/10.1038/s44182-025-00050-3.

Correspondence and requests for materials should be addressed to Hongyu Yu.

Reprints and permissions information is available at http://www.nature.com/reprints

Publisher's note Springer Nature remains neutral with regard to jurisdictional claims in published maps and institutional affiliations.